Eurasian Journal of Science Engineering and Technology

Research

EFFECT OF CALCINATION TEMPERATURE AND CA:EG RATIO ON TL AND OSL CURVE COMPONENTS OF NEIGHBORITE

Veysi GUCKAN[1,*]

[1]*Physics Department, Cukurova University, 01330, Saricam, Adana, Turkey*

ABSTRACT

This study reveals the differences created by varying calcination temperature and citric acid/ethylene glycol ratio (CA:EG) in thermoluminescence (TL) and optically stimulated luminescence (OSL) curves so that the Neighborite ($NaMgF_3$) compound synthesized using sol-gel can be used as a radiation dosimeter. While producing $NaMgF_3$ phosphors, four different calcination temperatures (700, 800, 900 and 1000 °C) were applied for the calcination process. Characterization analyzes of the samples were performed using X-ray diffraction (XRD) and Scanning electron microscopy (SEM). It was observed that the oxide phases in the crystal structure of the sample increased gradually with increasing calcination temperature. At 1000 °C, it was observed that the crystal structure of the sample was deformed and moved away from the aimed structure. Considering the signal intensities in the TL and OSL glow curves obtained after radiation exposure and the data in the characterization analyzes, the calcination temperature of 800 °C was determined as the optimum temperature. This calcination temperature was kept constant and the samples were reproduced by changing the CA:EG ratio in four different ways (2:4, 4:4, 8:4 and 16:4). By comparing all the sample, the samples with the best crystallization and the most suitable surface morphology were determined. In TL glow curves, it was observed that deep traps could be formed only in samples calcined at 800 °C. Likewise, it was observed from the OSL glow curves that the samples calcined at 800 °C had higher sensitivity. It has been stated that the low sensitivity of the samples calcined at high temperatures is due to the density of the oxide phases formed in the calcination process.

Keywords: Thermoluminescence, Optically stimulated luminescence, Neighborite, Calcination conditions, Computerized deconvolution, Sol-gel technique

1. INTRODUCTION

Perovskites, with their variable formulas, flexible structures, numerous unique properties, and efficacy in a wide range of applications, are becoming hotspots and are being studied extensively [1,2]. The first identified perovskite is CaTiO3 by Gustav Rose in 1839 is named after the mineralogist L. A. Perovski [3], and then its formula is found in numerous new forms, such as ABX3, A3B2X9, etc., where A and B are cations (A has a larger radius than B) and X is a halogen or oxygen anion is derived [4]. Perovskite materials with a wide variety of properties and wide applications can be produced from different compositions and structures [5–8]. For example, luminescent perovskites are used in lighting [9], displays [10], biological imaging [11] or sensing [12], while some photoelectric perovskites are used in areas such as electrocatalysis [13] and photo-catalysis [14]. While the fields of use of perovskites with magnetic properties are magnetic cooling [15], information storage [16], biomedical imaging [17]; electrical perovskites are used to prepare ionic conductors [18], dielectric devices [19], etc. As we approach the present date, it is observed that researchers have done a lot of research into the luminescence in solid-state perovskites. The oldest known of these comes from a Chinese text published in the Song dynasty. Among these studies, luminescent perovskites have important applications in the fields of solar cells [20], lighting devices [21], scintillators [22], electronic devices; such as capacitors [23] or converters [24] or radiation dosimeters [25,26] . It would be helpful for readers to read some review articles for more information [27–29].

The mineral $NaMgF_3$, a material with a perovskite structure, was named Neighborite after the work of geologist Frank Neighbor, and then Chao and his colleagues described this mineral crystallographically [30]. O'Keefe and colleagues noted the structural similarity between NaMgF3 and MgSiO3 in the late 1970s [31]. Zhao and colleagues have done extensive work by studying the phase transitions [32] changing with temperature, and the structure of NaMgF3 [33]. NaMgF3 crystallizes into an orthorhombic crystal system and is identified in the space group Pcmn. It has a tetragonal structure between 760 and 900 oC and above 900 oC the unit cell becomes cubic [30].

The researchers stated that NaMgF3 has an effective atomic number (Zeff=10.4) close to the tissue equivalent and is a host compound that can be used for optical radiation dose estimation by OSL and RL methods, especially when used with lanthanide ions. It has been observed by some researchers that NaMgF3, which had many luminescence studies before, exhibited some

* Corresponding author, e-mail: veysiguckan@gmail.com (V. Guckan)
Recieved: 11.04.2022 Accepted: 07.06.2022
doi: 10.55696/ejset.1101711

interesting photoluminescence properties with divalent or trivalent lanthanides. In addition to the luminescence of trivalent lanthanides such as Pr [34], Er [35], Ce [36], Eu [37], Sm [38], Yb [39], Gd [40] and Dy [41], divalent lanthanides such as Sm [42,43], Yb [44] and Eu [45] were also reported.

In generally, $NaMgF_3$ is prepared using solid-state reactions. However, direct melting of the constituent fluorides has also been used. Simpler new techniques such as the solvothermal method, two-stage wet chemical methods have also been used recently. Fluoride salts are used as precursors in high-temperature techniques. Due to the ability of chlorine ions to prevent hydrolysis, some wet chemical methods that lead to the formation of OH-free fluorides are also preferred. It is necessary to remove traces of water to avoid parasitic oxyfluoride phases and thermal treatment should be in a reductive atmosphere. We obtained $NaMgF_3$ phosphors containing different activators by sol-gel method from metal fluoride solutions.

In this study, optimization studies were carried out for the variables (calcination temperature and CA:EG ratio) in the production process of the $NaMgF_3$ material, which was examined by some researchers for its use in the field of radiation dosimetry and stated to have superior dosimetric properties and very bright TL and OSL signals. $NaMgF_3$ microparticles with fluoride-based perovskite structure were obtained in laboratory conditions by Sol-gel method. For $NaMgF_3$, where no such optimization was found, the differences in calcination temperature and citric acid ratio in structure and luminescence efficiency were tested. It is thought that the optimization studies of the calcination temperature in this study will shed light on future dosimetric studies while investigating the effect of both TL and OSL signals. In this study, in which the difference in luminescence efficiency with the differences created by the calcination temperature in the host matrix was revealed, the differences in both TL and OSL curves were revealed by changing the CA:EG ratio. In addition, the luminescence efficiency of the doped $NaMgF_3$ samples produced using the optimized calcination temperature and CA:EG ratio is also presented.

2. MATERIAL AND METHOD

2.1. Sample preparation

In this study, the $NaMgF_3$ (Neighborite) sample as perovskite-type fluorides was synthesized using the sol-gel technique. $NaMgF_3$ polycrystal powder were prepared using the polycrystalline compound of NaF *(≥99.0%, Sigma Aldrich)* and MgF_2 *(≥99.99%, Sigma-Aldrich)* inappropriate proportions. Ethylene glycol (EG) solution *($C_2H_6O_2$, 99.8%, Sigma-Aldrich)* and citric acid (CA) *($C_6H_8O_7$, 99.5%, Sigma-Aldrich)* were used as a solvent and a reactant, respectively, with four different CA:EG ratios *(2:4, 4:4, 8:4 and 16:4).* The calcination process was performed using a high-temperature furnace at four different temperatures *(700, 800, 900 and 1000 °C)* for 2 h. To keep oxidation to a minimum and to prevent oxide formation, the oxygen level was reduced by passing argon gas through the furnace chamber during calcination process.

2.2. Luminescence measurements

Thermoluminescence and optically stimulated luminescence readouts were performed using a RisØ DA-20 TL/OSL reader system. This reader has a 90Sr–90Y beta source with the 6.689 Gy/min dose rate and 2.27 MeV maximum energy. All luminescence signals were recorded with a bialkaline photomultiplier tube (PMT) unit and Schott BG-39 (330-620 nm VIS range) and Hoya U 340 (290-390 nm UV range) filters placed in front of it. The luminescent samples were first irradiated with a beta dose of 0.2 Gy and then TL read-outs were performed from room temperature up to 500 °C. OSL readings were performed using the blue light source with a wavelength of 470 nm for 100 seconds of continuous stimulation (CW-OSL). All TL readouts and OSL pre-heatings were performed at 5 $°Cs^{-1}$ heating rate.

3. RESULTS AND DISCUSSION

3.1. Structural Analysis

3.1.1. XRD

$NaMgF_3$ microparticles were successfully produced in laboratory conditions using the sol-gel method. The inconsistencies in TL and OSL curves obtained after the production stage and the different dose responses of different batches were problematic, and more consistent results were aimed by obtaining optimum conditions with the variables of calcination temperature and CA:EG ratio. In this way, the opportunity to test the luminescence efficiency with varying calcination temperatures and CA:EG mol ratios was occurred. Figure 1a presents the X-ray diffraction patterns of $NaMgF_3$ samples obtained using the sol-gel method and calcined at four different calcination temperatures ranging from 700 to 1000 °C. After the calcination temperature was determined, the CA:EG variable was tested at 2:4, 4:4, 8:4 and 16:4 ratios. The XRD patterns of the $NaMgF_3$ microparticles obtained as a result of the production, in which the CA:EG ratios vary, are given in Figure 1b. As seen in the figure, it was

observed that the characteristic $NaMgF_3$ peaks as well as small oxide peaks increased with the increase of calcination temperature. However, it was observed that the structure was completely destroyed at 1000 °C or a different structure was formed unlike the $NaMgF_3$ phase. It is observed in the TL and OSL curves that the luminescence efficiency also decreases sharply with the deterioration of the structure (see Figure 3a and 4a). Different CA:EG mole ratios were compared in samples produced at 800 °C calcination temperature. The samples in which both the crystallization was better than the others (see Figure 1) and especially the OSL signals were the most intense (see Figure 4) were the $NaMgF_3$ microparticles produced in a 2:4 mole ratio. Miller indices of the main crystal structure of all the $NaMgF_3$ samples obtained except 1000 °C calcination temperature were indicated for the peaks associated with $NaMgF_3$ reported in the ICSD card numbered as ICSD:98-009-4085 and matched well with its Pnma space group with orthorhombic structure. In order to minimize oxidation and prevent the formation of oxide phases, the calcination process was carried out in an argon atmosphere. However, since the calcination process was carried out in a non-completely isolated high temperature furnace, this could not be prevented. Several oxide phases not mentioned here, for example MgO, were observed in the crystal structure.

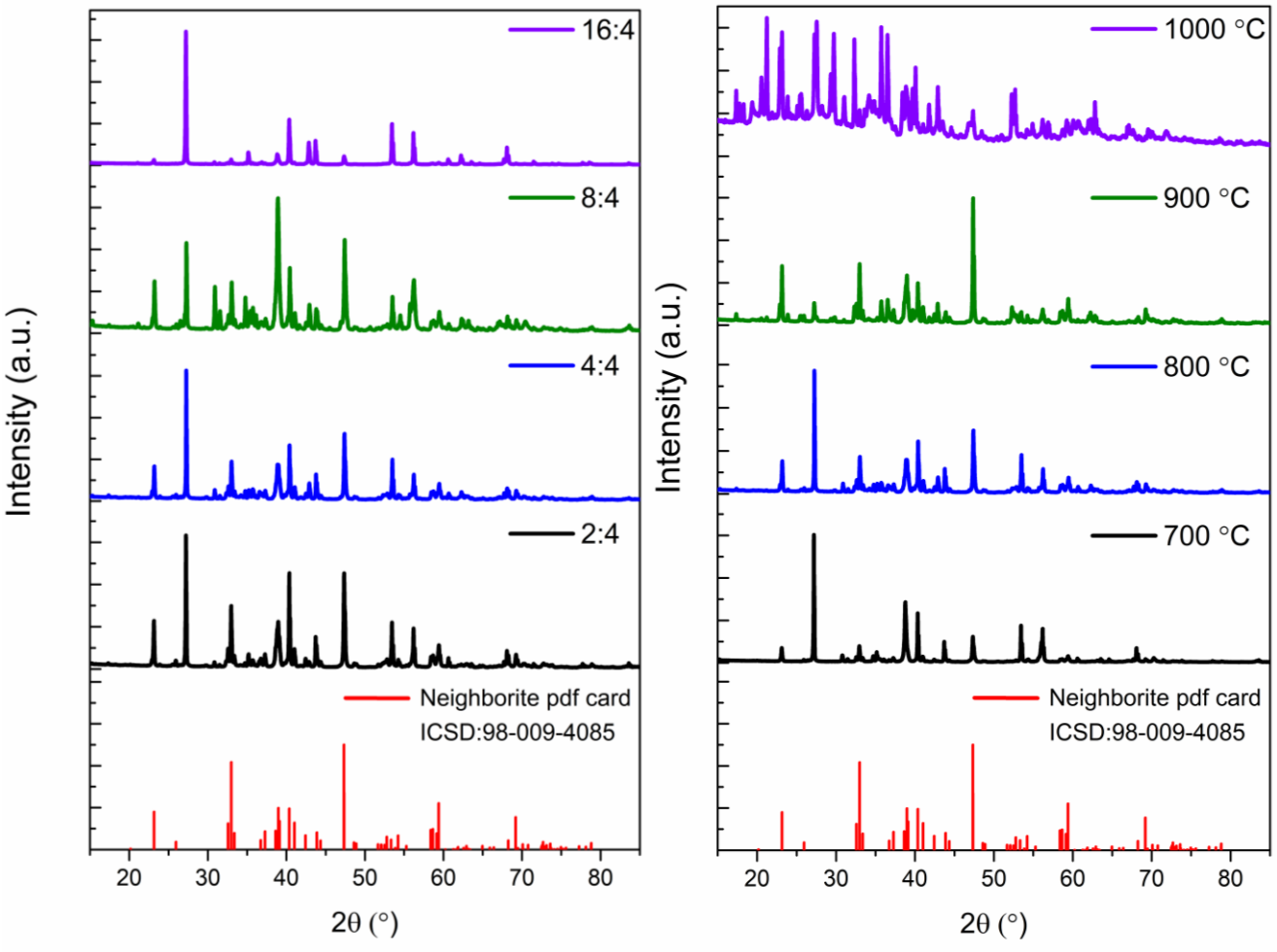

Figure 1. XRD patterns of $NaMgF_3$ microparticles synthesized using the sol-gel methods with different calcination temperatures and CA:EG molar ratios.

3.1.2. SEM

The surface morphology of $NaMgF_3$ fluoroperovskite was analyzed with SEM analysis at different magnifications of 5000 and 10000x. A series of SEM images of $NaMgF_3$ microparticles obtained with calcination conditions (700, 800, 900 and 1000 °C) and CA:EG molar ratios (2.4, 4:4, 8:4 and 16:4) were recorded. Increasing calcination temperatures in the $NaMgF_3$ structure improved the crystallinity of powders. SEM images reveal that the microparticles exhibit a self-repetitive image in a continuous distribution for all samples. (Figure 2a). In the SEM images obtained after the constant calcination temperature of 800 °C of the

samples produced at different CA:EG ratios, it was observed that the homogeneous morphology on the surface in all case (see Figure 2b).

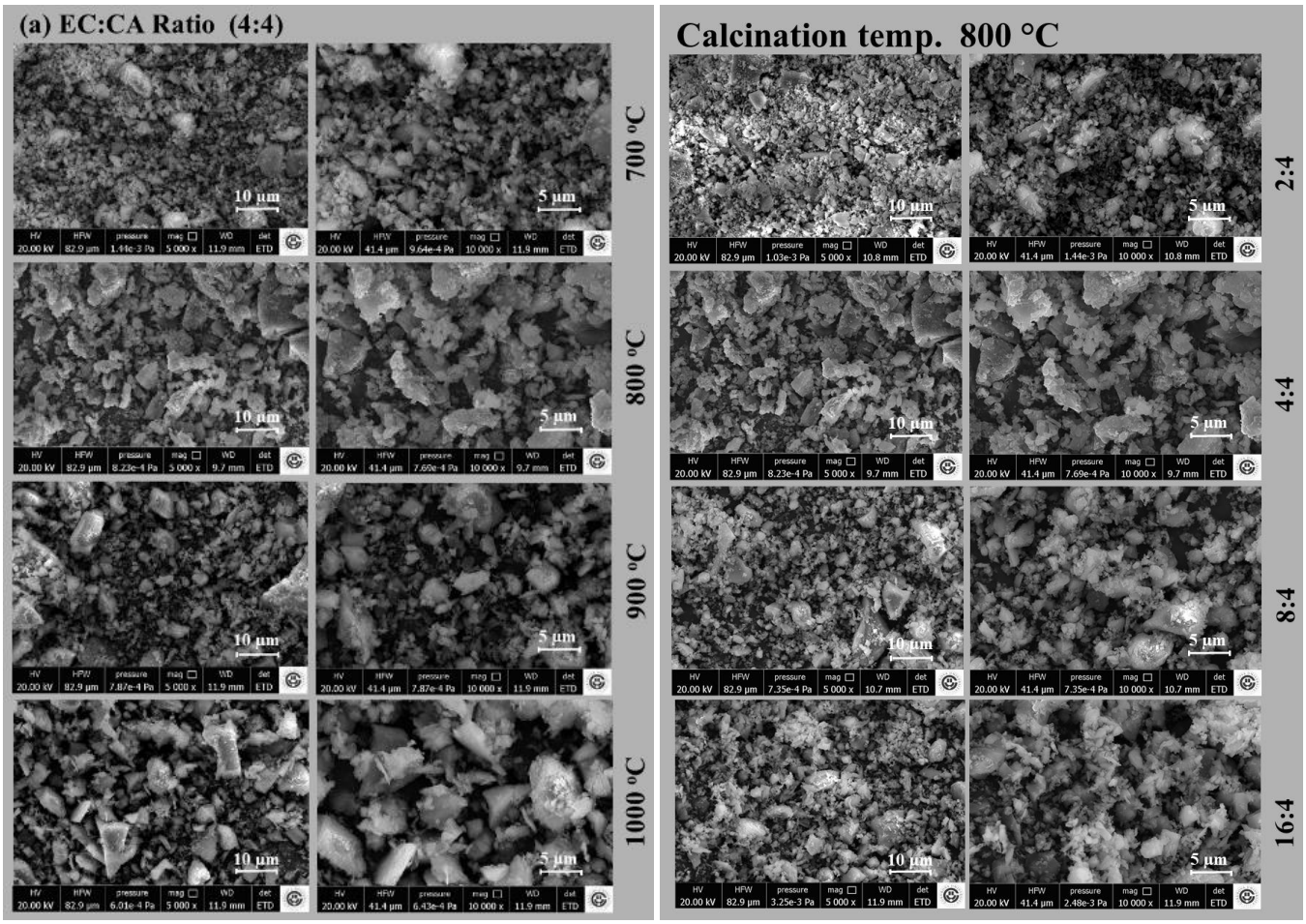

Figure 2. SEM images of the $NaMgF_3$ samples prepared using sol-gel method (a) calcined at different temperature and (b) prepared in different CA:EG molar ratios.

3.2. Luminescence characterization

3.2.1. TL glow curve analysis

TL glow curves of undoped $NaMgF_3$ obtained using the sol-gel method are given in Figures 3a and 3b. As can be seen from the TL glow curves due to different calcination temperatures, TL peaks were observed at around 75 and 120 °C with different intensities depending on the trap groups of $NaMgF_3$ phosphorus. Unlike the others, there was another broad TL peak, which appeared weaker than the other peaks between 225 and 360 °C under the 800 °C calcination condition. In generally, TL peaks located at high temperatures in TL glow curves of dosimeters are preferred because they indicate deeper traps than those at lower temperatures and relatively more stable signals are obtained from these traps. In such a case, the optimum calcination temperature was chosen as 800 °C. And then, by keeping this temperature constant, $NaMgF_3$ phosphor was reproduced with the four different ratios of CA-EG. It can be clearly seen that the 4:4 ratio of the CA:EG exhibits higher intensity TL signals than the others and can create deep traps. It should be noted that the TL glow curves here were recorded with a Schott BG-39 VIS band pass filter with transmittance in the visible region (330-620 nm).

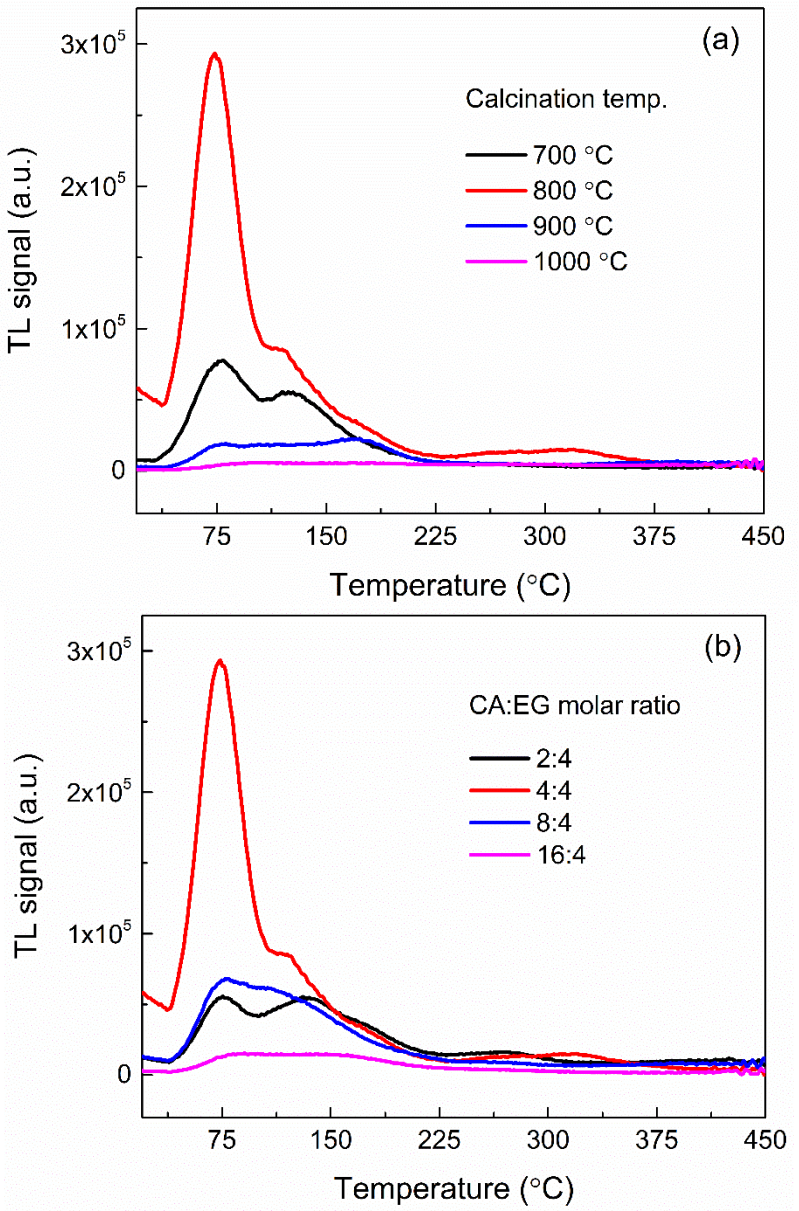

Figure 3. TL glow curves of $NaMgF_3$ differing with varying (a) calcination temperature and (b) CA:EG ratio. TL glow curves were recorded by heating from room temperature to 450 °C without preheating, and each TL glow curve presented was obtained by averaging the TL signals recorded from 3 samples.

The computerized glow curve deconvolution technique (CGCD) was used with the help of the Microsoft Excel spreadsheet [46] can be used for the analysis of the complex TL curves which have overlapping peaks. The kinetic parameters such as E_a, s, and b were calculated assuming the general order kinetic which is described by Kitis et al. [47]. The components which they are created in the TL glow curve are given in Figure 4. Goodness of fit value as Figure of Merit (FOM) was determined as 2.23%. Calculated kinetic parameters E_a, s, and b values were shown in Table 1. Activation energies were observed to have an increasing tendency between 0.76 and 1.17 eV. The frequency factors corresponding to the peaks were determined between 10^8-10^{10} s^{-1}. The lifetimes τ of the traps were calculated using Equation 1 [48] as 2.45 minutes, 1.30 hours, 5.15 days, 4.50 years and 1.50x10^3 years, respectively.

$$\tau = s^{-1} exp\left(\frac{E}{kT}\right) \quad (1)$$

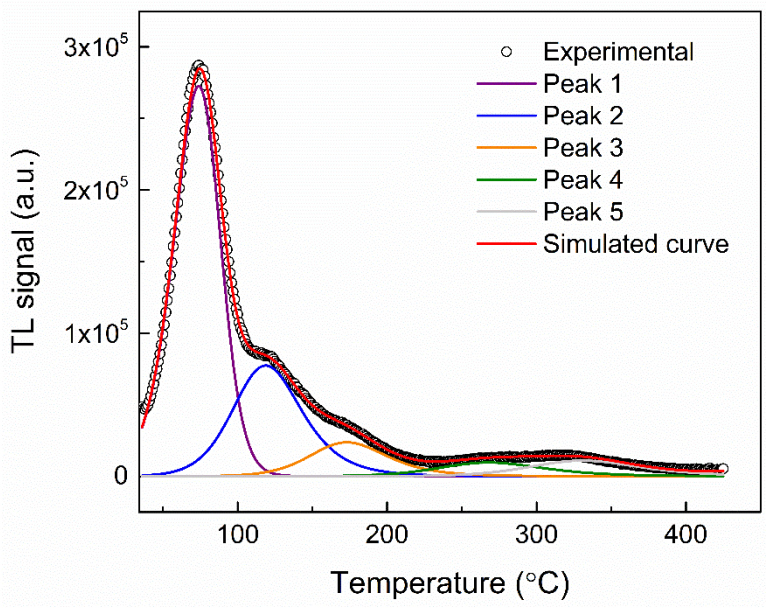

Figure 4. Deconvoluted TL glow curve from undoped $NaMgF_3$ using sol-gel method calcined at 800 °C with the CA:EG ratio of 4:4.

Table 1. Kinetic parameters obtained from deconvoluted TL glow curve

	T_{max} (°C)	E(eV)	s (Hz)	b (a.u.)	τ	FOM (%)
Peak 1	74	0.76	$3.38x10^{10}$	1.35	2.45 m	
Peak 2	118	0.80	$4.79x10^{9}$	2.00	1.30 h	
Peak 3	173	0.92	$6.15x10^{9}$	2.00	5.15 d	2.23
Peak 4	267	0.99	$2.94x10^{8}$	2.00	4.50 y	
Peak 5	330	1.17	$1.04x10^{9}$	2.00	$1.50x10^{3}$ y	

3.2.2. Continuous-wave OSL decay curve analysis

The OSL decay curves of the $NaMgF_3$ phosphors were recorded using 100 s blue light stimulation from samples calcined at different calcination temperatures with different ratio of CA:EG. The recorded OSL decay curves after 100 °C preheating of the $NaMgF_3$ samples are compared in Figure 5. Figure 5a presents the OSL signals of $NaMgF_3$ samples calcined at different calcination temperatures as a function of time. It was observed that the samples calcined at 800 °C gave the most intense OSL signals. This is thought to be due to the fact that the $NaMgF_3$ phase is formed more smoothly at 800 °C than the others and that different oxide phases are less common in the crystal structure. Figure 5b presents the OSL signals of $NaMgF_3$ samples produced with different CA:EG molar ratios and calcined at 800 °C as a function of time. Here, it was observed that the samples produced with the CA:EG ratio of 2:4 gave the most intense OSL signals among them.

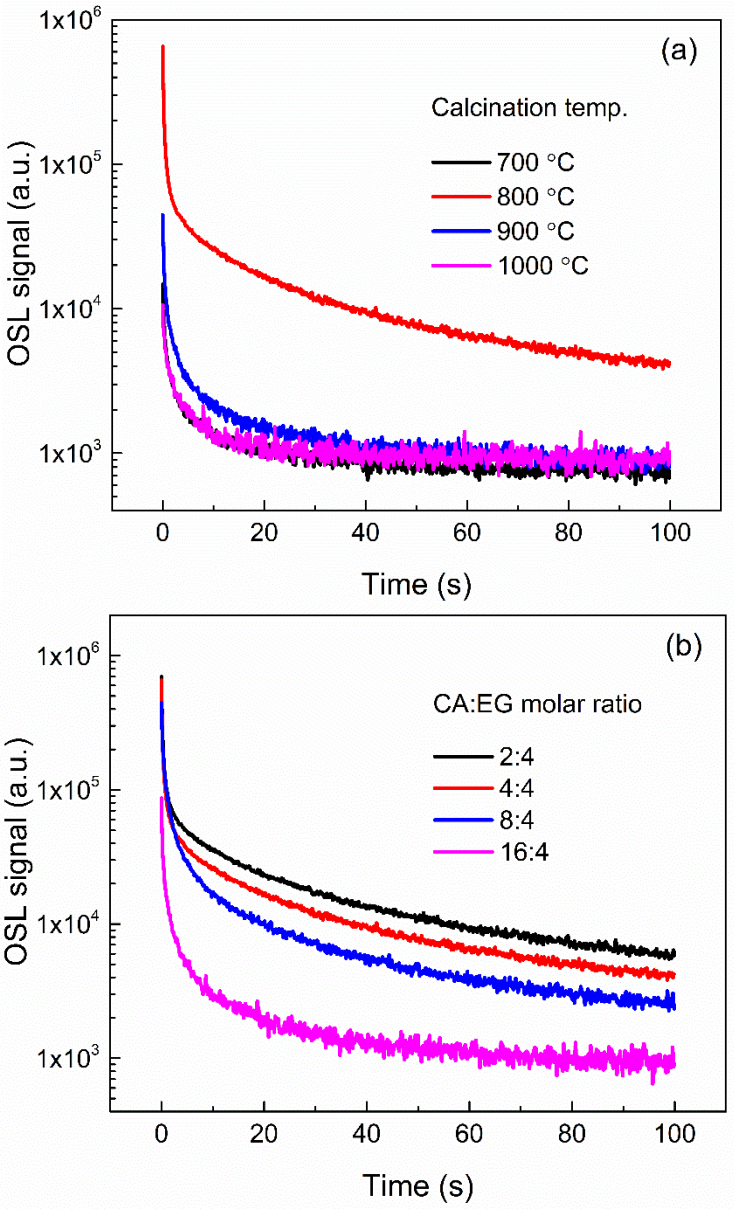

Figure 5. OSL decay curves of the NaMgF3 phosphors prepared using sol-gel method (a) at different calcination temperatures and (b) using different CA:EG ratios. OSL curves were recorded by blue light stimulation after 100 °C preheating, and each OSL decay curve presented was obtained by averaging the OSL signals recorded from 3 samples.

The CW-OSL decay curve of all $NaMgF_3$ samples were analyzed using the fitting method according to time decaying functions (see Figure 6) approximated by general-order which can be written as follows;

$$I\,(t) = bkg + I_1\left[1 + (b_1 - 1)\frac{t}{\tau_1}\right]^{-\frac{b_1}{b_1-1}} + I_2\left[1 + (b_2 - 1)\frac{t}{\tau_2}\right]^{-\frac{b_2}{b_2-1}} + \cdots \quad (2)$$

where, each component is named as fast, medium and slow component, respectively, according to their lifer times $\tau_{1,2,3}$ values. $I(t)$ is the OSL intensity as a function of time, $I_{1,2,3..}$ are the amplitudes, t is the stimulation time and bkg is the background signal of the reader. The decay of the undoped $NaMgF_3$ samples prepared with different conditions were characterized by a fast initial decay and then the medium and a slower decay. The fitting curves for all the undoped $NaMgF_3$

samples estimated using the three components were statistically found well. The related kinetic parameters and FOM value are given in Table 2.

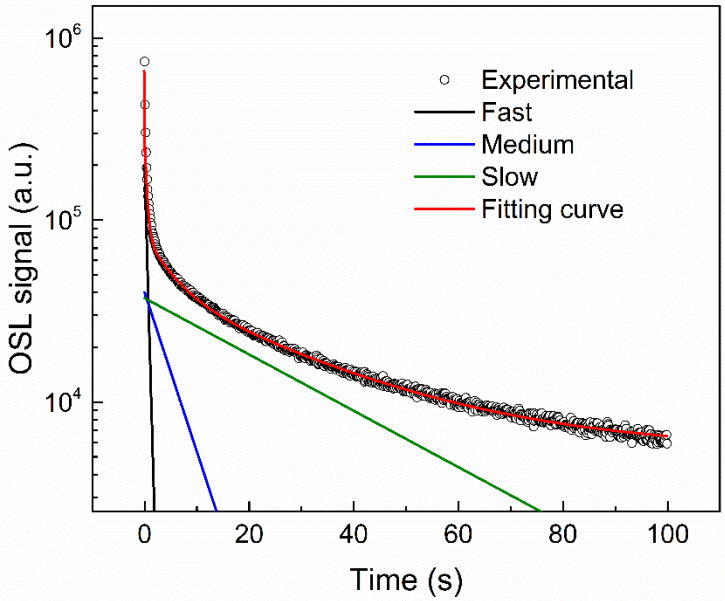

Figure 6. The OSL decay curve of the undoped $NaMgF_3$ calcined at 800 °C with the CA:EG ratio of 2:4 and its fast, medium and slow components.

Table 2. Decay constants for fast, medium and slow components of the OSL decay curve of $NaMgF_3$.

		Fast		**Medium**		**Slow**			
		A1	t1	A2	t2	A3	t3	bkg	FOM
CA:EG	Temp.								
4:4	700 °C	4853.87	0.46	2689.24	2.82	887.37	18.58	793.22	2.14
	800 °C	180917.70	0.38	32811.33	4.22	26785.06	25.25	3807.55	2.01
	900 °C	13861.43	0.42	7038.30	2.66	1763.43	19.26	936.01	2.35
	1000 °C	2323.34	0.45	2608.24	3.13	481.1763	18.38	920.05	2.96
Temp.	CA:EG								
800 °C	4:2	200588.01	0.43	40062.94	4.96	37222.76	28.06	543.50	1.76
	4:4	180917.70	0.38	32811.33	4.22	26785.06	25.25	3807.55	2.01
	4:8	137440.70	0.62	50339.46	3.34	15867.50	23.42	2307.60	2.11
	4:16	21923.39	0.47	10701.47	2.83	2858.22	18.69	989.36	2.86

4. CONCLUSION

In this study, $NaMgF_3$ samples were produced successfully with the uncommon sol-gel production technique. In XRD diffraction patterns, it is observed that the crystal structure gradually deteriorates due to the increasing calcination temperature and at the same time, different oxide phases increase. At the calcination temperature of 1000 °C, it is seen that the structure has completely deteriorated. This was an expected situation [30]. Obtained $NaMgF_3$ samples except 1000 °C are reported in the ICSD card numbered ICSD:98-009-4085 and fit well with the orthorhombic structure in Pnma space group. The complexity of the surface morphology (possibly due to the presence of oxide phases) makes it pointless to observe the effect of varying calcination temperature or CA:EG ratio. It is seen that TL peaks at low temperature are more intense in TL glow curves taken from samples obtained under different conditions. It was observed that high temperature TL peaks were obtained only in $NaMgF_3$

samples calcined at 800 °C and with a CA:EG ratio of 4:4, and the kinetic parameters of this curve were estimated by the CGCD method. Its activation energies of the traps corresponding to each TL peak were observed to have an increasing tendency between 0.76 and 1.17 eV. The situation did not change much in the OSL decay curves taken from the $NaMgF_3$ samples. Only $NaMgF_3$ samples calcined at 800 °C and with CA:EG ratios of 2:4 or 4:4 had high-intensity. The decay constants with its fast, medium and slow components of these OSL curves were estimated using fitting curve method.

This study reveals the changes in TL and OSL curves with changing calcination conditions and CA:EG ratio in the use of $NaMgF_3$ samples for dosimetric purposes, and the kinetic parameters that change depending on these changes. It is suggested that $NaMgF_3$ phosphorus has a high potential as a radiation dosimeter and should be investigated further for this purpose, and it is thought that this study will shed light on future studies.

SIMILARTY RATE: 19%

ACKNOWLEDGEMENT

I would like to thank Prof. Dr. Zehra YEGINGIL for the opportunities and valuable opinions she provided.

This research is sponsored by NATO's Emerging Security Challenges Division in the framework of "The Science for Peace and Security Programme (SPS)". Financial assistance from the NATO SPS MYP under the research contract number G5647 are acknowledged. I would like to thank the Cukurova University Research Projects Development and Coordination Unit under FUA-2021-13936 are gratefully acknowledged.

REFERENCES

[1] Y. Zhang, W. Jie, P. Chen, W. Liu, J. Hao, Y. Zhang, P. Chen, W. Liu, W. Jie, J. Hao, Ferroelectric and Piezoelectric Effects on the Optical Process in Advanced Materials and Devices, Advanced Materials. 30 (2018) 1707007. https://doi.org/10.1002/ADMA.201707007.

[2] Y. Wei, Z. Cheng, J. Lin, An overview on enhancing the stability of lead halide perovskite quantum dots and their applications in phosphor-converted LEDs, Chemical Society Reviews. 48 (2019) 310–350. https://doi.org/10.1039/C8CS00740C.

[3] Z. Cheng, J. Lin, Layered organic–inorganic hybrid perovskites: structure, optical properties, film preparation, patterning and templating engineering, CrystEngComm. 12 (2010) 2646–2662. https://doi.org/10.1039/C001929A.

[4] Z. Zeng, Y. Xu, Z. Zhang, Z. Gao, M. Luo, Z. Yin, C. Zhang, J. Xu, B. Huang, F. Luo, Y. Du, C. Yan, Rare-earth-containing perovskite nanomaterials: design, synthesis, properties and applications, Chemical Society Reviews. 49 (2020) 1109–1143. https://doi.org/10.1039/C9CS00330D.

[5] R. Saha, A. Sundaresan, C.N.R. Rao, Novel features of multiferroic and magnetoelectric ferrites and chromites exhibiting magnetically driven ferroelectricity, Materials Horizons. 1 (2013) 20–31. https://doi.org/10.1039/C3MH00073G.

[6] W.J. Yin, B. Weng, J. Ge, Q. Sun, Z. Li, Y. Yan, Oxide perovskites, double perovskites and derivatives for electrocatalysis, photocatalysis, and photovoltaics, Energy & Environmental Science. 12 (2019) 442–462. https://doi.org/10.1039/C8EE01574K.

[7] L. Wang, H. Zhou, J. Hu, B. Huang, M. Sun, B. Dong, G. Zheng, Y. Huang, Y. Chen, L. Li, Z. Xu, N. Li, Z. Liu, Q. Chen, L.D. Sun, C.H. Yan, A Eu 3+ -Eu 2+ ion redox shuttle imparts operational durability to Pb-I perovskite solar cells, Science (1979). 363 (2019) 265–270. https://doi.org/10.1126/SCIENCE.AAU5701/SUPPL_FILE/AAU5701_WANG_SM.PDF.

[8] X. Zhang, Z. Li, H. Zhang, S. Ouyang, Z. Zou, Luminescence properties of Sr2ZnWO6:Eu3+ phosphors, Journal of Alloys and Compounds. 469 (2009) L6–L9. https://doi.org/10.1016/J.JALLCOM.2008.01.117.

[9] J.S. Yao, J. Ge, B.N. Han, K.H. Wang, H. bin Yao, H.L. Yu, J.H. Li, B.S. Zhu, J.Z. Song, C. Chen, Q. Zhang, H.B. Zeng, Y. Luo, S.H. Yu, Ce3+-Doping to Modulate Photoluminescence Kinetics for Efficient CsPbBr3 Nanocrystals Based Light-Emitting Diodes, J Am Chem Soc. 140 (2018) 3626–3634. https://doi.org/10.1021/JACS.7B11955/SUPPL_FILE/JA7B11955_SI_001.PDF.

[10] Y. Cheng, C. Shen, L. Shen, W. Xiang, X. Liang, Tb3+, Eu3+ Co-doped CsPbBr3 QDs Glass with Highly Stable and Luminous Adjustable for White LEDs, ACS Applied Materials and Interfaces. 10 (2018) 21434–21444. https://doi.org/10.1021/ACSAMI.8B05003/SUPPL_FILE/AM8B05003_SI_001.PDF.

[11] M. Pellerin, E. Glais, T. Lecuyer, J. Xu, J. Seguin, S. Tanabe, C. Chanéac, B. Viana, C. Richard, LaAlO3:Cr3+, Sm3+: Nano-perovskite with persistent luminescence for in vivo optical imaging, Journal of Luminescence. 202 (2018) 83–88. https://doi.org/10.1016/J.JLUMIN.2018.05.024.

[12] T. Addabbo, F. Bertocci, A. Fort, M. Gregorkiewitz, M. Mugnaini, R. Spinicci, V. Vignoli, Gas sensing properties of YMnO3 based materials for the detection of NOx and CO, Sensors and Actuators B: Chemical. 244 (2017) 1054–1070. https://doi.org/10.1016/J.SNB.2017.01.054.

[13] G. Chen, Y. Zhu, H.M. Chen, Z. Hu, S.F. Hung, N. Ma, J. Dai, H.J. Lin, C. te Chen, W. Zhou, Z. Shao, An Amorphous Nickel–Iron-Based Electrocatalyst with Unusual Local Structures for Ultrafast Oxygen Evolution Reaction, Advanced Materials. 31 (2019) 1900883. https://doi.org/10.1002/ADMA.201900883.

[14] E. Grabowska, Selected perovskite oxides: Characterization, preparation and photocatalytic properties—A review, Applied Catalysis B: Environmental. 186 (2016) 97–126. https://doi.org/10.1016/J.APCATB.2015.12.035.

[15] B. Arun, V.R. Akshay, G.R. Mutta, C. Venkatesh, M. Vasundhara, Mixed rare earth oxides derived from monazite sand as an inexpensive precursor material for room temperature magnetic refrigeration applications, Materials Research Bulletin. 94 (2017) 537–543. https://doi.org/10.1016/J.MATERRESBULL.2017.07.006.

[16] Y. Cao, S. Cao, W. Ren, Z. Feng, S. Yuan, B. Kang, B. Lu, J. Zhang, Magnetization switching of rare earth orthochromite CeCrO3, Applied Physics Letters. 104 (2014) 232405. https://doi.org/10.1063/1.4882642.

[17] X. Chen, J. Song, X. Chen, H. Yang, X-ray-activated nanosystems for theranostic applications, Chemical Society Reviews. 48 (2019) 3073–3101. https://doi.org/10.1039/C8CS00921J.

[18] T. Asano, A. Sakai, S. Ouchi, M. Sakaida, A. Miyazaki, S. Hasegawa, Solid Halide Electrolytes with High Lithium-Ion Conductivity for Application in 4 V Class Bulk-Type All-Solid-State Batteries, Advanced Materials. 30 (2018) 1803075. https://doi.org/10.1002/ADMA.201803075.

[19] X. Liu, N. Kent, A. Ceballos, R. Streubel, Y. Jiang, Y. Chai, P.Y. Kim, J. Forth, F. Hellman, S. Shi, D. Wang, B.A. Helms, P.D. Ashby, P. Fischer, T.P. Russell, Reconfigurable ferromagnetic liquid droplets, Science (1979). 365 (2019) 264–267. https://doi.org/10.1126/SCIENCE.AAW8719/SUPPL_FILE/AAW8719S9.MP4.

[20] C.M. Sutter-Fella, Y. Li, M. Amani, J.W. Ager, F.M. Toma, E. Yablonovitch, I.D. Sharp, A. Javey, High Photoluminescence Quantum Yield in Band Gap Tunable Bromide Containing Mixed Halide Perovskites, Nano Letters. 16 (2016) 800–806. https://doi.org/10.1021/ACS.NANOLETT.5B04884/SUPPL_FILE/NL5B04884_SI_001.PDF.

[21] Y. Kim, E. Yassitepe, O. Voznyy, R. Comin, G. Walters, X. Gong, P. Kanjanaboos, A.F. Nogueira, E.H. Sargent, Efficient Luminescence from Perovskite Quantum Dot Solids, ACS Applied Materials and Interfaces. 7 (2015) 25007–25013. https://doi.org/10.1021/ACSAMI.5B09084/SUPPL_FILE/AM5B09084_SI_001.PDF.

[22] M.D. Birowosuto, D. Cortecchia, W. Drozdowski, K. Brylew, W. Lachmanski, A. Bruno, C. Soci, X-ray Scintillation in Lead Halide Perovskite Crystals, Scientific Reports 2016 6:1. 6 (2016) 1–10. https://doi.org/10.1038/srep37254.

[23] H. Yokoi, N. Wakiya, K. Shinozaki, N. Mizutani, Dielectric Properties and its Frequency Dependence of BaTiO3 Thin Film Single-Layer Capacitor that is Applicable to Multilayer Structure, Key Engineering Materials. 269 (2004) 229–232. https://doi.org/10.4028/WWW.SCIENTIFIC.NET/KEM.269.229.

[24] I. Dursun, C. Shen, M.R. Parida, J. Pan, S.P. Sarmah, D. Priante, N. Alyami, J. Liu, M.I. Saidaminov, M.S. Alias, A.L. Abdelhady, T.K. Ng, O.F. Mohammed, B.S. Ooi, O.M. Bakr, Perovskite Nanocrystals as a Color Converter for Visible Light Communication, ACS Photonics. 3 (2016) 1150–1156. https://doi.org/10.1021/ACSPHOTONICS.6B00187/SUPPL_FILE/PH6B00187_SI_001.PDF.

[25] V. Guckan, D. Kaya, V. Altunal, A. Ekicibil, F. Karadag, A. Ozdemir, Z. Yegingil, Impact of Li concentration in KMgF3:Eu,Yb fluoroperovskite on structure and luminescence properties, Journal of Alloys and Compounds. 902 (2022) 163810. https://doi.org/10.1016/J.JALLCOM.2022.163810.

[26] Z. Li, X. An, X. Cheng, X. Wang, … H.Z.-C., undefined 2014, First-principles study of the electronic structure and optical properties of cubic Perovskite NaMgF3, Iopscience.Iop.Org. (n.d.). https://iopscience.iop.org/article/10.1088/1674-1056/23/3/037104/meta (accessed April 10, 2022).

[27] X. Li, F. Cao, D. Yu, J. Chen, Z. Sun, Y. Shen, Y. Zhu, L. Wang, Y. Wei, Y. Wu, H. Zeng, All Inorganic Halide Perovskites Nanosystem: Synthesis, Structural Features, Optical Properties and Optoelectronic Applications, Small. 13 (2017) 1603996. https://doi.org/10.1002/SMLL.201603996.

[28] D.B. Mitzi, Templating and structural engineering in organic–inorganic perovskites, Journal of the Chemical Society, Dalton Transactions. 0 (2001) 1–12. https://doi.org/10.1039/B007070J.

[29] D. Chen, X. Chen, Luminescent perovskite quantum dots: synthesis, microstructures, optical properties and applications, Journal of Materials Chemistry C. 7 (2019) 1413–1446. https://doi.org/10.1039/C8TC05545A.

[30] E.C.T. Chao, H.T. Evans Jr, B.J. Skinner, C. Milton, Neighborite, NaMgF3, a new mineral from the green river formation, South Ouray, Utah, American Mineralogist: Journal of Earth and Planetary Materials. 46 (1961) 379–393.

[31] M. O'Keeffe, J.O. Bovin, Solid Electrolyte Behavior of NaMgF3: Geophysical Implications, Science (1979). 206 (1979) 599–600. https://doi.org/10.1126/SCIENCE.206.4418.599.

[32] K.S. Knight, G.D. Price, J.A. Stuart, I.G. Wood, High-temperature structural phase transitions in neighborite: A high-resolution neutron powder diffraction investigation, Physics and Chemistry of Minerals. 42 (2015) 45–52. https://doi.org/10.1007/S00269-014-0698-5/FIGURES/3.

[33] Y. Zhao, D.J. Weidner, J. Ko, K. Leinenweber, X. Liu, B. Li, Y. Meng, R.E.G. Pacalo, M.T. Vaughan, Y. Wang, A. Yeganeh-Haeri, Perovskite at high P-T conditions: An in situ synchrotron X ray diffraction study of NaMgF3 perovskite, Journal of Geophysical Research: Solid Earth. 99 (1994) 2871–2885. https://doi.org/10.1029/93JB02757.
[34] N.J.M. le Masson, A.P. Vink, P. Dorenbos, A.J.J. Bos, C.W.E. VanEijk, J.P. Chaminade, Ce3+ and Pr3+5d-energy levels in the (pseudo) perovskites KMgF3 and NaMgF3, Journal of Luminescence. 101 (2003) 175–183. https://doi.org/10.1016/S0022-2313(02)00411-8.
[35] Y.P. Du, Y.W. Zhang, Z.G. Yan, L.D. Sun, S. Gao, C.H. Yan, Single-Crystalline and Near-Monodispersed NaMF3 (M=Mn, Co, Ni, Mg) and LiMAlF6 (M=Ca, Sr) Nanocrystals from Cothermolysis of Multiple Trifluoroacetates in Solution, Chemistry – An Asian Journal. 2 (2007) 965–974. https://doi.org/10.1002/ASIA.200700054.
[36] S. Watanabe, T. Ishii, K. Fujimura, K. Ogasawara, First-principles relativistic calculation for 4f–5d transition energy of Ce3+ in various fluoride hosts, Journal of Solid State Chemistry. 179 (2006) 2438–2442. https://doi.org/10.1016/J.JSSC.2006.04.040.
[37] J.J. Schuyt, G.V.M. Williams, Oxygen-impurity charge transfer in NaMgF3:Ln (Ln = Yb, Sm, or Eu): Establishing the lanthanide energy levels in NaMgF3, Journal of Luminescence. 211 (2019) 413–417. https://doi.org/10.1016/J.JLUMIN.2019.04.004.
[38] J.J. Schuyt, G.V.M. Williams, Radiation-induced changes in the optical properties of NaMgF3(Sm): Observation of resettable Sm radio-photoluminescence, Materials Research Bulletin. 106 (2018) 455–458. https://doi.org/10.1016/J.MATERRESBULL.2018.06.039.
[39] J. Zhang, J. Wang, J. Xie, L. Wang, Q. Zhang, Enhancement of upconversion luminescence intensity in NaMgF3:2.5%Yb3+, 0.5%Er3+ nanocrystals with Eu3+ doping, Journal of Materials Science: Materials in Electronics. 32 (2021) 20882–20890. https://doi.org/10.1007/S10854-021-06604-Z/FIGURES/8.
[40] M. Venkata Narayana, K. Somaliah, L.H. Brixner, Thermally stimulated luminescence of gadolnium-activated NaMgF3 at 77 K, Crystal Research and Technology. 25 (1990) K209–K213. https://doi.org/10.1002/CRAT.2170250921.
[41] J.J. Schuyt, G.V.M. Williams, Photoluminescence of Dy3+ and Dy2+ in NaMgF3:Dy: A potential infrared radiophotoluminescence dosimeter, Radiation Measurements. 134 (2020) 106326. https://doi.org/10.1016/J.RADMEAS.2020.106326.
[42] J.J. Schuyt, G.V.M. Williams, Quenching of the Sm2+ luminescence in NaMgF3:Sm via photothermal ionization: Alternative method to determine divalent lanthanide trap depths, Applied Physics Letters. 115 (2019) 181104. https://doi.org/10.1063/1.5122669.
[43] J.C. Gâcon, A. Gros, H. Bill, J.P. Wicky, New measurements of the emission spectra of Sm2+ in KMgF3 and NaMgF3 crystals, Journal of Physics and Chemistry of Solids. 42 (1981) 587–593. https://doi.org/10.1016/0022-3697(81)90107-4.
[44] H. Nalumaga, J.J. Schuyt, R.D. Breukers, G.V.M. Williams, Radiation-induced changes in the photoluminescence properties of NaMgF3:Yb nanoparticles: Yb3+ → Yb2+ valence conversion and oxygen-impurity charge transfer, Materials Research Bulletin. 145 (2022) 111562. https://doi.org/10.1016/J.MATERRESBULL.2021.111562.
[45] V.S. Singh, P.D. Belsare, S. v. Moharil, Synthesis, characterization, and luminescence studies of rare-earth-activated NaMgF3, Luminescence. 37 (2022) 89–96. https://doi.org/10.1002/BIO.4149.
[46] D. Afouxenidis, G.S. Polymeris, N.C. Tsirliganis, G. Kitis, Computerised curve deconvolution of TL/OSL curves using a popular spreadsheet program, Radiation Protection Dosimetry. 149 (2012) 363–370. https://doi.org/10.1093/RPD/NCR315.
[47] G. Kitis, J.M. Gomez-Ros, J.W.N. Tuyn, Thermoluminescence glow-curve deconvolution functions for first, second and general orders of kinetics, Journal of Physics D: Applied Physics. 31 (1998) 2636. https://doi.org/10.1088/0022-3727/31/19/037.
[48] V. Pagonis, G. Kitis, C. Furetta, Numerical and practical exercises in thermoluminescence, (2006). Numerical and practical exercises in thermoluminescence. Springer Science & Business Media, 2006.